



OPEN

Effect of additive oxygen gas on cellular response of lung cancer cells induced by atmospheric pressure helium plasma jet

SUBJECT AREAS:
BIOLOGICAL PHYSICS
APOPTOSISHea Min Joh¹, Ji Ye Choi², Sun Ja Kim¹, T. H. Chung¹ & Tae-Hong Kang²Received
17 July 2014Accepted
26 September 2014Published
16 October 2014Correspondence and
requests for materials
should be addressed to
T.H.C. (thchung@dau.
ac.kr)¹Department of Physics, Dong-A University, Busan 604-714, Republic of Korea, ²Department of Biological Science, Dong-A University, Busan 604-714, Republic of Korea.

The atmospheric pressure helium plasma jet driven by pulsed dc voltage was utilized to treat human lung cancer cells *in vitro*. The properties of plasma plume were adjusted by the injection type and flow rate of additive oxygen gas in atmospheric pressure helium plasma jet. The plasma characteristics such as plume length, electric current and optical emission spectra (OES) were measured at different flow rates of additive oxygen to helium. The plasma plume length and total current decreased with an increase in the additive oxygen flow rate. The electron excitation temperature estimated by the Boltzmann plot from several excited helium emission lines increased slightly with the additive oxygen flow. The oxygen atom density in the gas phase estimated by actinometry utilizing argon was observed to increase with the additive oxygen flow. The concentration of intracellular reactive oxygen species (ROS) measured by fluorescence assay was found to be not exactly proportional to that of extracellular ROS (measured by OES), but both correlated considerably. It was also observed that the expression levels of p53 and the phospho-p53 were enhanced in the presence of additive oxygen flow compared with those from the pure helium plasma treatment.

Atmospheric pressure plasmas have drawn a considerable attention due to their potential in biomedical applications including bacterial sterilization, blood coagulation, dermatology, wound healing, and cancer treatment^{1–7}. Various effects of atmospheric pressure plasma on living cells have been demonstrated^{8–12}. Of particular interest are the plasma interactions with cancerous cells. It has been shown by several groups that the plasma is able to induce cell death (the programmed cell death, apoptosis or the necrotic cell rupture) in a number of cancer cell types^{7,13–20}. Among these, the induction of apoptosis by plasma treatment has proven an intriguing issue. The reactive oxygen species (ROS) produced by plasma are considered to be the key constituents that induce apoptosis²¹. The production of ROS such as superoxide (O_2^-), hydrogen peroxide (H_2O_2), oxygen atom (O), and hydroxyl radical (OH) in atmospheric pressure plasmas may affect the concentration of ROS inside the cells during the plasma-cell interactions. Although a moderate increase of ROS may induce cell proliferation, excessive amounts of ROS can cause damage to lipids, proteins, DNA, and a variety of cellular responses including cell cycle arrests, senescence, and apoptosis induction^{21–23}.

ROS can either be generated exogeneously or produced intracellularly from different sources. Plasma-induced ROS in the gas phase could result in intracellular ROS generation and apoptotic cell death. In our previous study, it was found that intracellular ROS generation was increased by the plasma treatment and the apoptosis rate correlated well with the levels of the intracellular and extracellular ROS^{16,24,25}. Over the past few years, a considerable number of studies have tried to increase the ROS in atmospheric pressure plasma medium for plasma biomedical applications. Many research groups have studied atmospheric pressure plasmas based on helium with only small fractions of oxygen (less than 5%) in order to increase concentrations of ROS and prevent plasma instability simultaneously²⁶. It is believed that He/O₂ plasmas are a good source of reactive oxygen species.

In this paper, the characteristics of atmospheric pressure He/O₂ plasma jet are studied. The plume length, current, and optical emission spectra (OES) are measured at different oxygen concentrations. Since the oxygen atom plays an important role in the plasma-living tissues interaction, the oxygen atom density is determined by the actinometry using a small amount of argon. In order to use the actinometry technique one needs to know the electron temperature. The electron temperature is estimated by the excitation temperature, which is calculated from the Boltzmann plot of several excited helium emission lines.

This paper examines the intracellular ROS concentration and DNA damage in plasma-exposed lung cancer cells (A549). Numerous investigations suggest that p53 acts to regulate the intracellular redox state and induces



apoptosis and plays a major role in the cellular response to the DNA damage by a pathway that is dependent on ROS production^{22,27,28}. To elucidate the biochemical effects of oxygen addition to the pure helium plasma, the intracellular ROS concentration, DNA damage response, and the expression level of p53 in plasma-exposed cancer cells were investigated.

Experiment

Atmospheric-pressure helium/oxygen plasma jet device. The structure of the jet device and the changes in the plasma plume lengths for different type of oxygen injection are shown in Figure 1. The plasma jet consists of two electrodes, Teflon fitting, a quartz confinement tube, and a funnel-shaped nozzle. At the center of the quartz tube, a stainless steel capillary tube was used as the power electrode. The small diameter of the capillary electrode with a sharp edge allows for the local enhancement of the electric field and thus, a considerable reduction in the breakdown voltage compared to that for the plasma jets utilizing the annular ring electrode or dielectric barrier discharge jets, while providing a stable room-temperature operation²⁹. Aluminum foil strip was used as the ground electrode³⁰. Two types of oxygen injection were compared for effective plasma treatment of living cells. One has He/O₂ admixture gas channel (Type 1) and the other has a separated gas channel (Type 2).

Experimental setup with diagnostic system. The plasma was generated by the pulsed dc-driven source with a repetition frequency of several tens of kilohertz (FTLab PDS 4000). The working gas (helium) was delivered at a flow rate 1 L/min and the reactive gas (oxygen) flow rates were varied from 0 to 100 SCCM. The waveforms of the voltage and current were measured using a real time digital oscilloscope (Lecroy WS44XS-A) via high voltage probe (Tektronix P5100) and current monitor (Pearson 4100). To confirm the reactive species generated by the plasma jet in the open air and to verify the increase of oxygen atom in the plasma, the emission spectra of the atmospheric pressure plasma jet were monitored using a fiber optic spectrometer (OceanOptics USB-2000 + XR-ES). The optical emission from the plasma is collected using a 400- μ m-diameter fiber

placed in front of the discharge. Since the O-containing radicals play a key role in the plasma-cell interaction, the effect of additive oxygen gas on the emission intensities from oxygen atom and O-containing radicals was also explored. The ozone density was measured by the ozone detector (Interscan Corp. 4000 Series digital compact portable analyzer) in front of the plasma jet. The distance between the ozone detector and the plasma jet was 10 mm.

Results and Discussion

Lengths of plasma plume. Admixture of helium and oxygen has been widely used to produce more radicals in atmospheric pressure plasma jets^{31–33}. The results indicate that, when a small amount of oxygen is introduced, the plasma plume length decreases with increasing the oxygen concentrations. Adding oxygen into the feeding gas tends to diminish the production of radicals due to the electron attachment to oxygen inside the nozzle³⁴. In this work, two types of oxygen injection were used to determine a proper addition method suitable for effective plasma treatment. The measured plume lengths, indicating the distance many reactive species can extend into the ambient atmosphere, are shown as functions of applied voltage and additive oxygen flow rate in Fig. 2. In accordance with previous reports, our results show that the plasma plume length decreases with increasing the oxygen flow rate³⁰. As the applied voltage was increased and oxygen gas flow rate decreased, the plasma plume length increased. Especially, the plume length was reduced gradually in Type 2 (Figure 2B) compared to in Type 1 (Figure 2A) with oxygen flow rate. The Type 1-mixing (direct mixing of helium and oxygen) interferes with each gas flow essential for the discharge stability and requires much higher breakdown voltage due to the presence of oxygen molecules. In Type 2, on the other hand, the helium and oxygen gases are not mixed together before the ignition of helium plasma inside the discharge region. Accordingly, oxygen molecules interact with the helium plasma following the plasma ignition, which leads to relatively easy incorporation of oxygen molecules into the plasma state. Therefore, the use of the capillary tube (Type 2) is found to be favorable to mix the additive oxygen gas efficiently under a stable jet operation.

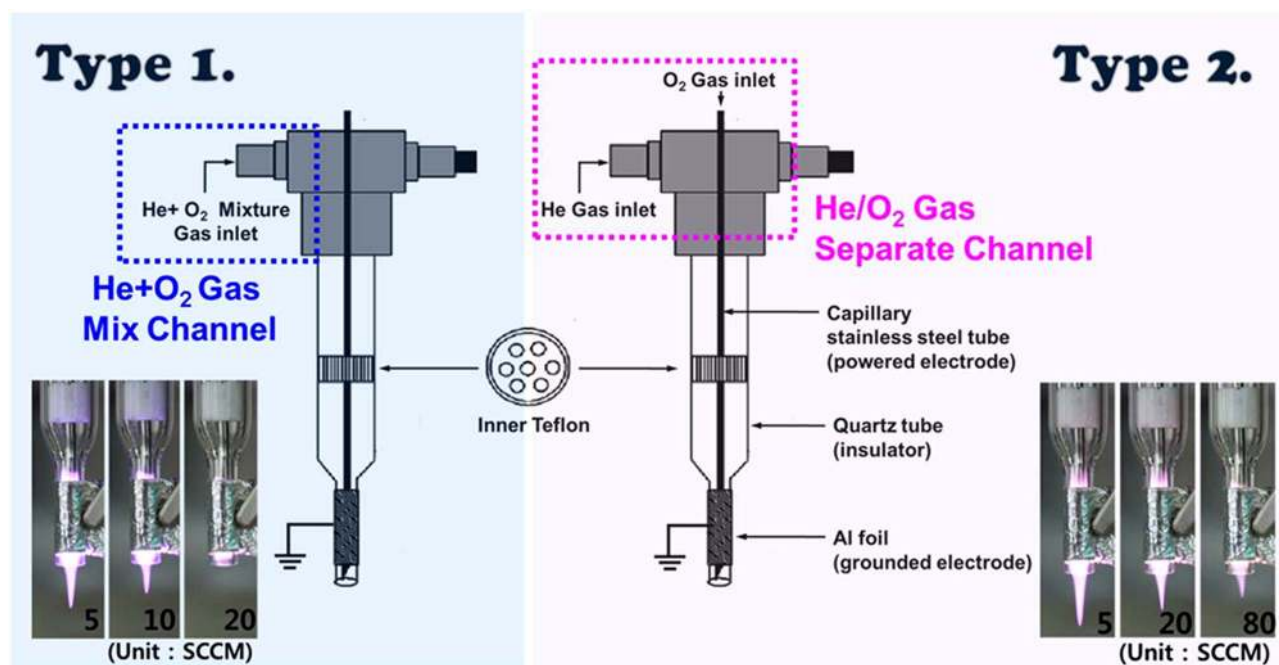


Figure 1 | Plasma jet device used to treat living cells. Structure of the jet devices and photographs of helium/oxygen plasma for different oxygen flow rates (Type 1: one channel with admixture gas, Type 2: a capillary tube acts as a separate channel for O₂ gas mixing). A typical operating condition of pulsed-dc plasma jet is the applied voltage 1.8 kV_{pp}, repetition frequency 50 kHz, and duty ratio 10%.

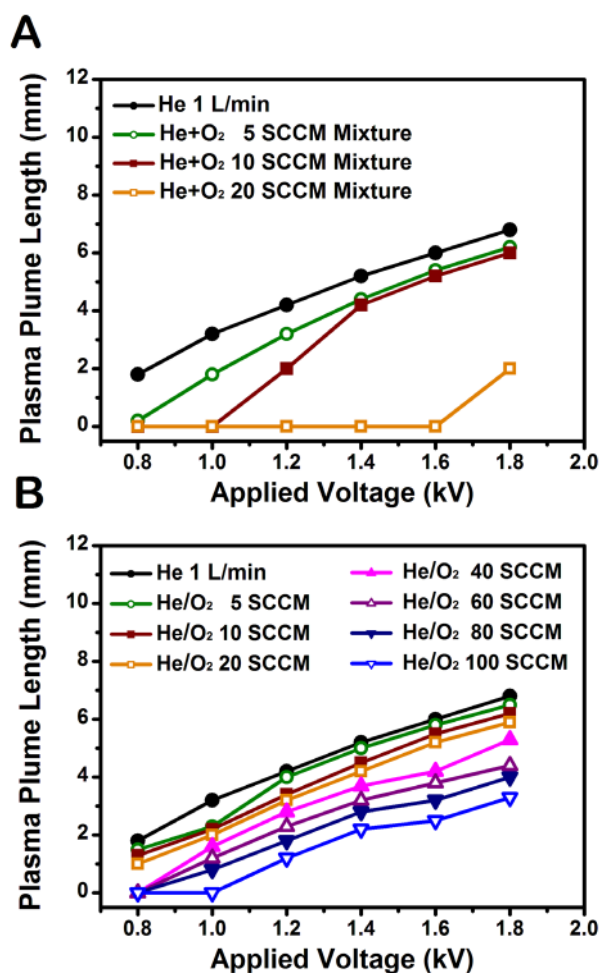


Figure 2 | Comparison of plasma plume lengths from two types of jet. Plume lengths as functions of applied voltage and additive oxygen flow rate (A) in Type 1 and (B) in Type 2. In Type 2, the plasma plume length was reduced gradually with oxygen flow rate compared to Type 1.

Electrical characteristics. The typical waveforms of the applied voltage and total current for the pulsed discharge operating at a repetition frequency of 50 kHz in Type 2 are shown in Figure 3A. Two distinct discharge current pulses per applied voltage pulse are observed. To find out the actual discharge current, the displacement current I_{no} (without gas flow, plasma off) is subtracted from the total current I_{tot} (plasma on). For the applied voltage amplitude 1.7 kV, the peak value of the primary discharge current is about 0.10 A and the peak value of the secondary discharge is smaller than that of the primary discharge. The secondary discharge ignites because of the voltage induced by the charges which have accumulated on the surface of the quartz tube during the primary discharge³⁰.

Figure 3B represents the total current as a function of oxygen concentration for two types of oxygen injection. This characteristic is similar to the change in the plasma plume length. In the type 1-mixing, when O₂ flow rate reaches 20 SCCM, the voltage and current characteristics were disturbed much in accordance with the change in the plume length shown in Figure 2A. As mentioned above, atmospheric pressure plasma jets based on the direct mixture of helium and oxygen require a higher applied voltage than pure helium plasma due to differing plasma ignition conditions, the type 1-mixing results in an inefficient plasma ignition. The oxygen molecules severely affect the initiation process of the helium plasma in Type 1.

Optical characteristics. Figure 4A shows typical emission spectrum observed in the He plasma jet with 10 SCCM oxygen flow through

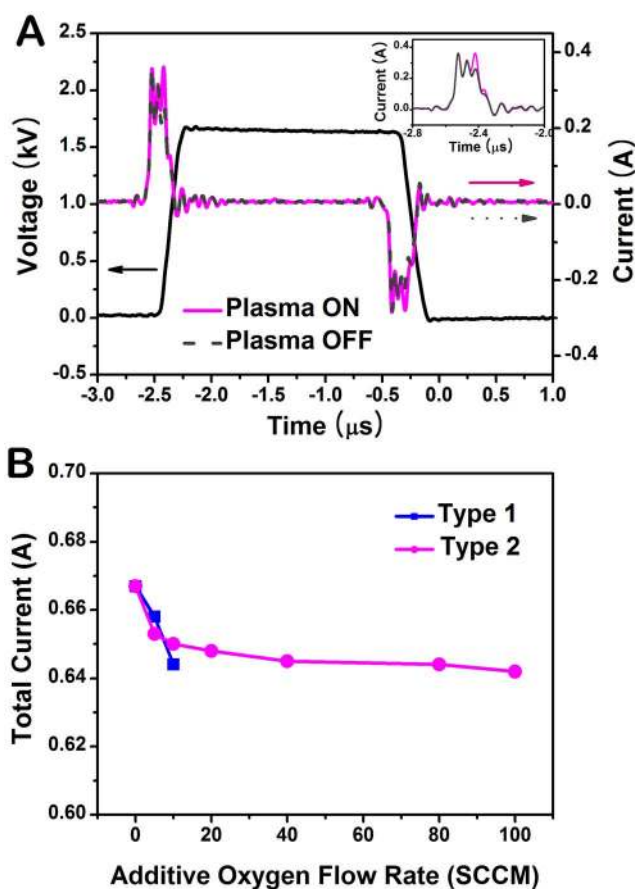


Figure 3 | Voltage-current characteristics of the discharge. (A) Typical waveforms of voltage (black solid line) and current in Type 2 jet. The operating condition of pulsed-dc plasma jet is the applied voltage 1.7 kV_{pp}, repetition frequency 50 kHz, and duty ratio 10%. The inset shows the total current (plasma on; pink solid line) and displacement current (plasma off; gray dashed line). To find out the actual discharge current, the displacement current is subtracted from the total current. (B) Total current as a function of additive oxygen flow rate for two types of oxygen injection.

the capillary electrode (Type 2). The discharge produces a significant UV radiation that belongs to transitions of the NO_y bands at 200–300 nm, the OH band at 308 nm, the atomic oxygen lines at 777 and 844 nm, the N₂ emission bands at 310–440 nm, and the N₂⁺ emission bands at 391–428 nm. Helium plasma jet with a separated oxygen channel was observed to produce more ROS in the plasma. This is attributed to the higher density of oxygen atom introduced in the excitation region. The variations of the intensities of NO, OH, H_x and O with additive oxygen flow are shown in Figure 4B. The intensities from these species decreased with additive oxygen flow except a slight increase of the intensity from O 844 nm at 10 SCCM. This is attributable to a decrease in the current with additive oxygen flow shown in Figure 3B. The plasma density can be estimated from the current assuming that the drift velocity is not much changed with additive oxygen flow. From the experimental results of the current and optical intensities, it can be inferred that the plasma density decreases with an increase in the oxygen flow. This is partly attributable to the reduction of electron density due to attachment to oxygen³⁵. It is noted that the addition of oxygen to the He plasma causes a decrease in the light emissions from He and air molecules. This suggests that some electrons are probably consumed to produce O radicals when O₂ is injected. Others then collide with air, water vapor, and He to produce N, OH, H_x and He radicals³⁴. This phenomenon is consistent with the changes in the plasma plume length and volume mentioned above. When the

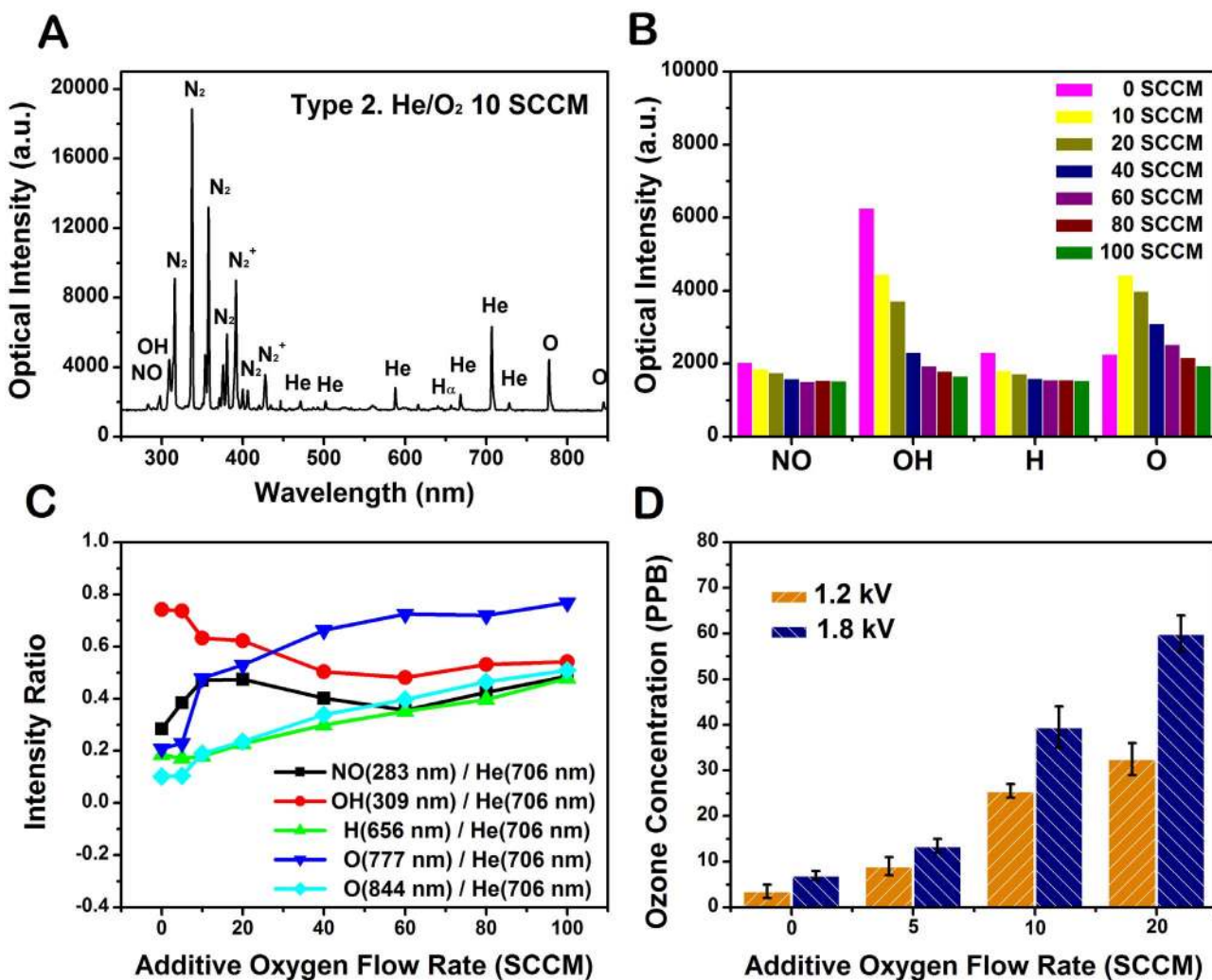


Figure 4 | Various reactive species and ozone monitoring in Type 2. (A) Optical emission spectrum of the plasma plume from 250 nm to 850 nm observed in the helium/oxygen plasma at the applied voltage 1.7 kV_{pp}, repetition frequency 50 kHz, and duty ratio 10%. (B) Comparisons of the change of the emission intensities from NO, OH, H, O radicals in different oxygen flow rates increasing from 0 to 100 SCCM. (C) The intensity ratios of the lines from NO, OH, H, O radicals to the helium line (706 nm). (D) Measurement of ozone concentration for different oxygen flow rates increasing from 0 to 20 SCCM.

oxygen flow rate is raised from 0 SCCM to 100 SCCM, the plume color becomes whitened due to the contributions from the light emission at diverse frequencies.

Figure 4C represents the optical emission intensity ratios of the lines from NO, OH, H, O radicals to the helium line (706 nm). Since the amount of He remains unchanged in the plasmas with different oxygen addition, the normalized intensities can represent the excited state densities of the species NO, OH, H, and O. The line intensities from NO and OH decreased with additive oxygen flow rate a little further than that of line intensity from He. On the other hand, the line intensities from O and H exhibit the opposite behavior. It is believed that the increased oxygen species in the plasma contributes to the cancer therapy due to its strong oxidative effect on the cells³⁶. Figure 4D shows the ozone production as a function of the additive oxygen flow rate. Ozone is a strong oxidant that generates ROS in cells and even causes DNA damage³⁷. During the plasma treatment, ozone levels increased with the oxygen flow rate. Ozone's damaging effect of the cell can be mediated via an induction of ROS within cells³⁸. Since the reaction $O + He + O_2 \rightarrow He + O_3$ is believed as the main way to produce ozone in the discharge region³⁹, it is expected that the ozone density correlates with the densities of atomic oxygen and oxygen molecule. Thus, the ozone density keeps growing with increase in the concentration of O₂⁴⁰.

Determination of excitation temperature & oxygen atom density.

The excitation temperature was estimated by using a Boltzmann plot method applied to several excited helium emission lines (447, 501, 587, 667, 706, and 728 nm)⁴¹. The atomic emission intensity (I_{pq}) of the transition from level p to level q depends on the transition probability (A_{pq}) and absolute population of the atomic level (n_p), as shown in the following equation; $I_{pq} = n_p A_{pq} h\nu$ (where h is the Planck constant and ν is the photon frequency corresponding to the $p \rightarrow q$ transition). Assuming a Boltzmann distribution of the population of the atomic level, the emission intensity is expressed as $I_{pq} \propto A_{pq} g_p h\nu \exp\left(-\frac{E_p}{k_B T_{exc}}\right)$ (where E_p and g_p are the energy and degeneracy of excited level p , respectively, k_B is the Boltzmann constant, and T_{exc} is the excitation temperature in Kelvin). From the measurement of intensity and wavelength, a Boltzmann plot was obtained for the helium plasma with 40 SCCM additive oxygen gas (Figure 5A). Using this formula, the electron excitation temperature can be estimated. Figure 5B shows that the measured excitation temperature is in the range of 0.22–0.26 eV. The excitation temperature slightly increased with the additive oxygen flow up to 60 SCCM. The presence of oxygen in the plasma, a source of electronegative species, causes an increase of the sustaining voltage



and the electric field strength. Therefore, the mean electron kinetic energy is increased and this leads to an increase of the excitation temperature⁴³. The excitation temperature may be used as a rough indicator of the electron temperature. Because it is free electrons which cause the excitation, their energies should be described by a Boltzmann distribution at a given temperature⁴¹. The electron temperature increases and the electron density decreases (inferred from the decrease in the optical intensities in Figure 4B) with increasing oxygen concentration. In this range, the contribution of Penning ionization decreases due to the reduction of the available helium metastables in the plasma. This observation is in agreement with the results of the global modeling⁴⁴.

O₂-containing plasmas are of interest in cancer therapy due to their ROS effect in cells. To examine the change in O-atom density, the fixed feed gas was kept constant at 1 L/min helium with 0.1% trace of argon admixtures (for actinometry) and the oxygen flow rates were varied from 0 to 100 SCCM. Optical emission actinometry is a widely utilized diagnostic tool for in-situ monitoring of spatial and temporal variations of atomic and molecular concentrations. In this method, a known concentration of an impurity is introduced, and the intensities of two neighboring spectral lines, one from the known gas and one from the sample, are compared. Since both species are bombarded by the same electron distribution and the concentration of the actinometer is known, the density of the sample can be calculated. To determine the concentration of the ground state oxygen atoms, O (3s ³P – 3p ³S) 844 nm and Ar (3p⁵ 4p (2p₁) – 3p⁵ 4s (1s₂)) 750.4 nm transitions were chosen and the dissociation fraction can be determined by calculating the ratio^{42,45,46}.

$$\frac{n_o}{n_{O_2}} = \frac{I_{ij}^o K_{ij}^{Ar} h\nu_{ij}^{Ar} A_{ij}^{Ar} k_e^{2p1} \sum_j A_{ij}^{3p} + k_Q^{3p} n_{O_2} n_{Ar}}{I_{ij}^{Ar} K_{ij}^{O} h\nu_{ij}^{O} A_{ij}^{O} k_e^{3p} \sum_j A_{ij}^{2p1} + k_Q^{2p1} n_{O_2} n_{Ar}} - \frac{k_{de}^{3p}}{k_e^{3p}} \quad (1)$$

Here, n_l is the number density of ground species l , I_{ij}^l is the intensity of emission from excited species l for the transition $i \rightarrow j$, A_{ij}^l is the Einstein coefficient, K_{ij}^l is the spectral response of the system, and ν_{ij}^l is the frequency of the light emission. And k_e^{3p} is the rate coefficient for electron-impact direct excitation to O* (3s ³P) from the ground-state O, k_e^{2p1} is the rate coefficient for electron-impact direct excitation to Ar (2p₁) from the ground-state Ar, k_{de}^{3p} is the rate coefficient for electron-impact dissociative excitation to O* (3s ³P) from the ground-state O₂, and k_Q is the rate coefficient for collisional quenching. The ratio of rate coefficients k_e^{2p1}/k_e^{3p} and k_{de}^{3p}/k_e^{3p} are obtained from the literature⁴². Neglecting the collisional quenching, the O-atom density is finally evaluated according to

$$n_o = \frac{I_{ij}^o h\nu_{ij}^{Ar} k_e^{2p1} a_{Ar}}{I_{ij}^{Ar} h\nu_{ij}^o k_e^{3p} a_o} n_{Ar} - \frac{k_{de}^{3p}}{k_e^{3p}} n_{O_2}, \quad (2)$$

where $a_i = A_{ik}^i/A_i^i (= \sum_k A_{ik}^i)$ is the optical decay rate of the upper state i of species l denotes the effective optical branching ratio of the transition. Figure 5C indicates that the ground state atomic oxygen density slightly increases with the oxygen flow rate. This result is in agreement with the global modeling⁴⁷. However, it should be noted that the estimation of ground state O-density utilizing Eq. (2) is not precise at the higher oxygen concentrations because non-negligible portion of the excited state atomic oxygen is generated by collisional reactions involving oxygen metastables and excited oxygen molecules^{40,44,47}. Then, the number density of O* (3s ³P), represented by $k_e^{3p} n_e a_o$ in the denominator of the first term in Eq. (2) (the electron density n_e is cancelled with the one in the numerator), increases actually with increase in the oxygen

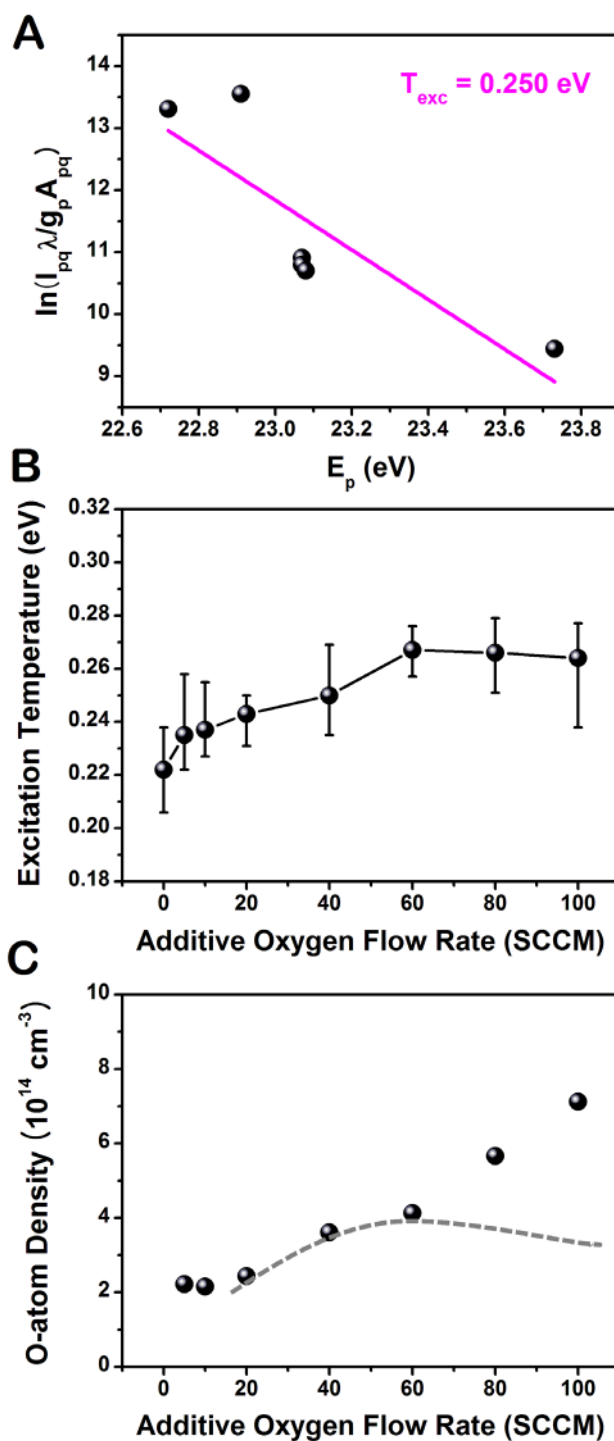


Figure 5 | Excitation temperature and oxygen atom density at different additive oxygen flows in Type 2. A Boltzmann plot method was used to estimate the excitation temperature: (A) Boltzmann plot of atomic helium lines (447, 501, 587, 667, 706, and 728 nm) for the additive oxygen flow rate of 400 SCCM. Variations of (B) the excitation temperature and (C) estimated atomic oxygen density via actinometry as a function of the additive oxygen flow rate. The dotted line indicates the expected estimates when the generation of excited oxygen atom via the collisional reactions involving oxygen metastables and excited oxygen molecules is considered.

concentration. Therefore, if this contribution is considered, the ground state O-density is likely to behave as indicated by the dot line in Figure 5C, which is in accord with the experimental results of rf-driven atmospheric pressure plasmas^{39,48}.



Plasma-cell interaction: intracellular ROS concentrations. To enhance the intracellular ROS generation in cells, the cells were treated by the helium plasma jet with additive oxygen gas. Figure 6A shows the fluorescence images (upper row) of intracellular ROS concentration in A549 cells (non-treated, He plasma-treated, He/O₂ plasma-treated) immediately after plasma treatment. The figures of lower row represent the bright-field images using an inverted microscopy. It is observed that plasma exposure leads to the increase of the intracellular ROS generation and plasma-induced ROS production can be controlled by additive oxygen gas. The highest intracellular ROS concentration in the plasma-treated cells was seen to occur at an additive oxygen flow rate of 20 SCCM, as shown in Figure 6B. Interestingly, when the oxygen flow rate was increased to 40 SCCM, a slight decrease in intracellular ROS concentration was observed. It means that high oxygen flow rate into the feeding gas influences the plasma discharge diminishing the production of radicals due to the electron attachment to oxygen inside the nozzle. Therefore, plasmas with higher oxygen flow rate than 40 SCCM tend to induce lesser intracellular ROS concentration. The generation of intracellular ROS is not solely determined by the atomic oxygen density but influenced by the concentrations of NO, OH, and O₃.

Plasma-cell interaction: DNA damage response. To elucidate the effect of cellular damage induced by plasma in cancer cells, the expression level of p53 in cells treated with plasma was investigated. The tumor suppressor protein p53 plays a major role in the cellular response to DNA damage and other genomic aberrations. DNA damage induces phosphorylation of p53 at Ser15 and Ser20. Activation of p53 can lead to cell cycle arrest and apoptosis by activating transcription of many downstream target genes^{27,28}. Reactive oxygen species have been considered as important mediators of the DNA damage after plasma treatment¹⁹. At 12 hours after plasma or plasma with oxygen treatment, expression level of p53 was significantly increased compared to those from the gas control (Figure 7A). Since the p53 activation is required for expression of itself we measured the level of phosphorylation of p53 at Ser15 (p-p53, the active form of p53) at 2 hours after the treatment and found that prominent p-p53 expression in plasma-treated cells (Figure 7B). In order to scrutinize the additional oxygen effect on p53 signaling in single cell level, we performed immunocytochemistry using p53 and p-p53 antibodies at 2 hours after the treatment. The results indicate that both the number of p53 and p-p53 positive cells and the fluorescence intensity in each of the oxygen-plasma treated cells were higher compared to those in the plasma only treated cells (Figure 7C & D), implicating more DNA damage accumulation by the additional oxygen in plasma.

In conclusion, the atmospheric pressure helium plasma jet driven by pulsed dc voltage was utilized to treat human lung cancer cells in vitro. Additive oxygen flow affects the plasma state, such as plasma plume length, total current, and optical emission intensities from the plasma species including He and oxygen-related radicals. It was observed that the properties of plasma plume can be adjusted by the injection type and flow rate of additive oxygen gas. To add oxygen gas efficiently, the use of the capillary tube for a separated channel-mixing was found to be favorable. With increase in the additive oxygen flow rate, the plasma plume length, total current, and optical emission intensities decreased. The admixture He/O₂ in atmospheric pressure plasma jet was found to be useful in enhancing the intracellular ROS concentrations in human lung cancer cells (A549). The concentration of intracellular ROS (measured by DCF-DA assay) was not exactly proportional to that of extracellular ROS (measured by OES), but both correlated considerably. The overproduction of ROS may partially contribute to DNA damage. He/O₂ plasma treatment on A549 cells resulted in the accumulation of the expression

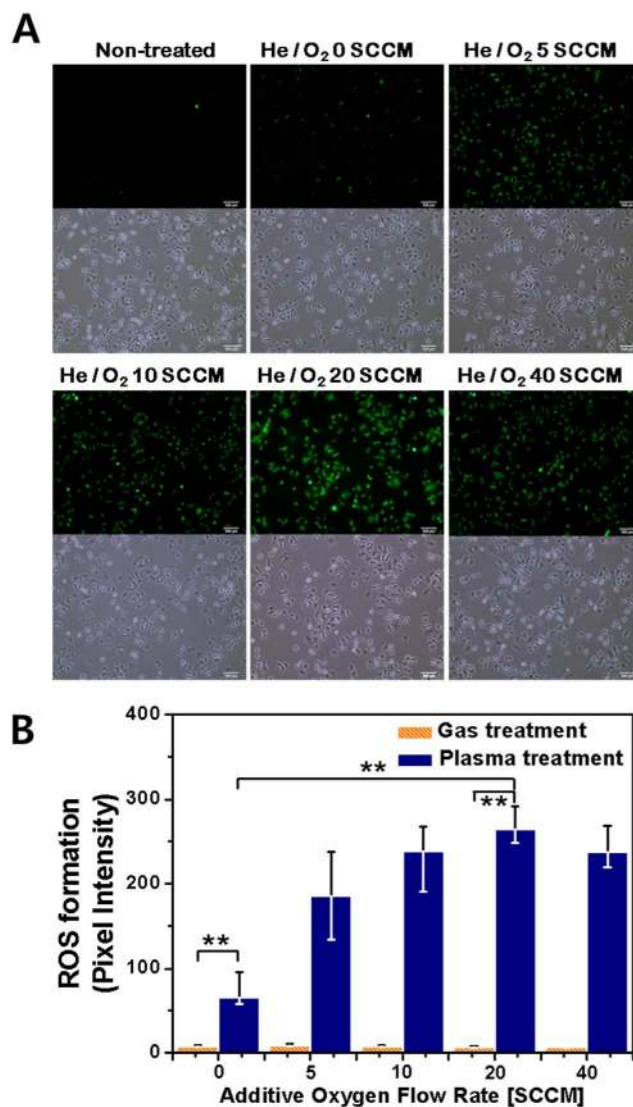


Figure 6 | Intracellular ROS in A549 cells following plasma treatment. A549 cells were treated with DCF-DA and assayed using fluorescence microscopy. Intracellular ROS formation in response to helium plasma-exposed A549 cells for different oxygen flow rate: (A) Fluorescence images (upper row) of intracellular ROS concentration in A549 cells (non-treated, He plasma-treated, He/O₂ plasma-treated) and bright-field images (lower row), (B) the quantification by measuring fluorescence pixel intensity with MetaMorph software (Each point represents the mean \pm SD of three replicates. * $p < 0.05$ and ** $p < 0.01$). Scale bar = 100 μ m.

and phosphorylation status of p53. Adding a small amount of oxygen to rare gas will cause a considerable progress in effectively inducing cancer cell death by atmospheric pressure plasma jets. The reported plasma device represents a valuable tool for ROS-promoting cancer therapy.

Methods

Cell culture. The interaction of the plasma jet with living cells was examined on human lung adenocarcinoma cell lines (A549). The cancer cells were transferred every 2–3 days to a new dish with fresh culture medium and incubated at 37°C with humidified air and 5% CO₂. The culture medium was composed of DMEM (Dulbecco's Modification of Eagle's Medium) with 10% fetal bovine serum (FBS) and 100 U/ml penicillin. For sample preparation, cells were trypsinized and transferred to 60-mm Petri dishes.

Plasma-cell interaction. The applied voltage, repetition frequency and duty ratio were 1.8 kV (or 1.6 kV), 50 kHz and 10%, respectively. The helium gas flow rate was 0.5 L/min for plasma-cell interactions. Such a reduced gas flow rate is advantageous

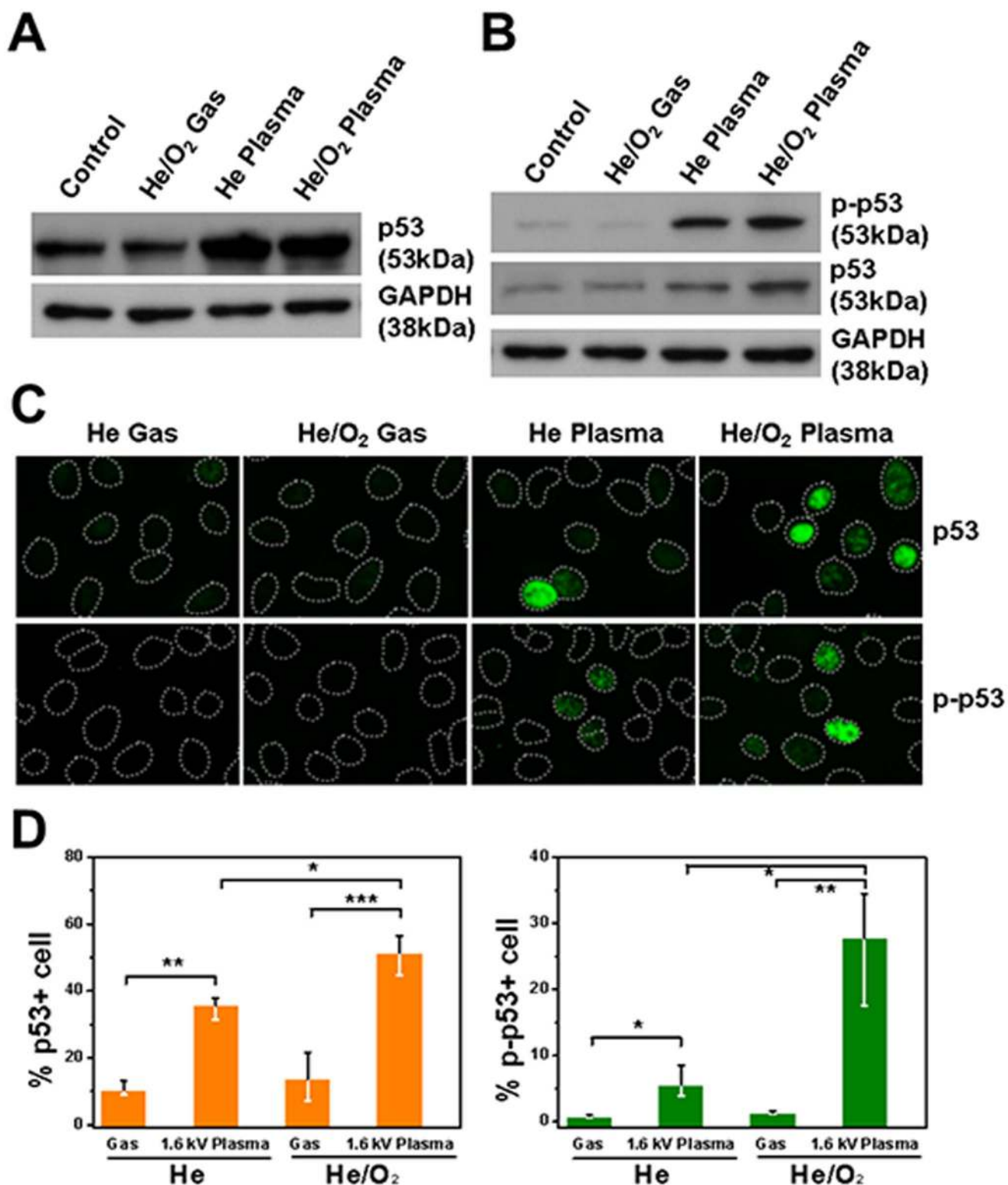


Figure 7 | Effect of plasma treatment on DNA damage in A549 cells. (A) Protein level of p53 at 12 h after the gas or plasma-treatment was analyzed using an immunoblot assay. GAPDH was probed to indicate the evenness of protein loading, (B) Immunoblottings of phospho-p53 (p-p53), p53 and GAPDH at 2 h after the indicated treatments. Uncropped full scans for A & B are shown in the Supplementary Figure 1. (C) Cells treated with indicated gas or plasma were fixed 2 hour later and immunostained for p53 and p-p53 (green), and DNA were counterstained with Hoechst dye (depicted as dotted lines), and (D) the quantification of (C) by measuring fluorescence pixel intensity (Each point represents the mean \pm SD of three replicates. * $p < 0.05$, * $p < 0.01$ and *** $p < 0.001$).

as it can limit damage by dehydration in sensitive cells and tissue samples. Then, cells were exposed to plasma (and/or gas flow only) for 10 s on nine (or twenty) designated points per dish. A distance from the nozzle to cell surface was adjusted as 5 mm for a direct contact between plasma plume and cells. During the plasma treatment, each dish contained a small amount (a few hundred microliters) of serum-free Hanks' balanced salt solution (HBSS) to prevent cell drying.

Measurement of intracellular ROS. Intracellular ROS assay is a cell-based assay for measuring reactive oxygen species activity within a cell. The assay employs the cell-permeable fluorogenic probe DCF-DA (Molecular Probes®), which diffuses into cells and is deacetylated by cellular esterases to the non-fluorescent DCFH. In the presence of ROS, DCFH is rapidly oxidized to highly fluorescent DCF⁵⁰. Generation of ROS can be detected by monitoring the increase in fluorescence. Fluorescence was measured



with excitation and emission wavelengths set at 488 nm and 520 nm, respectively. The A549 cells (10^6 cells) in dishes were pretreated with $10 \mu\text{M}$ DCF-DA for 5 min at 37°C in the dark. Intracellular ROS production was observed in the marked points. After helium/oxygen plasma treatment, cells were washed with phosphate buffered saline (PBS). Fluorescence-activated cells were detected using fluorescence microscopy (Nikon Japan) and quantified by measuring pixel intensity with Metamorph software (Molecular Devices, Sunnyvale, CA). Statistical analyses were performed using Prism software (Graphpad USA). Data are expressed as mean \pm SD. Comparisons between two groups were analyzed by Student's t-test, and trend over time was analyzed using one-way and two-way ANOVA.

Western blot analysis. The expression of proteins was evaluated using western blot analysis. Whole-cell lysates were prepared using $1 \times$ lysis buffer (Cell Signaling). The protein concentration was measured by using bicinchoninic acid (BCA) protein assay kit (Thermo Scientific). Equivalent amounts of protein ($40 \mu\text{g}$) from each lysate were resolved by 10% SDS-PAGE (sodium dodecyl sulfate polyacrylamide gel electrophoresis) gels, transferred to polyvinylidene difluoride (PVDF) membranes (Whatman) by electroblotting, and then probed with phospho-p53 (Ser 15), p53 and GAPDH (as a loading control) antibodies (all from Cell Signaling Technology). Membranes were incubated with secondary horseradish peroxidase (HRP)-conjugated antibody (Santa Cruz Biotechnology). Blots were developed using enhanced chemoluminescence (ECL; Pierce).

Immunocytochemistry. For immunofluorescence staining, A549 cells were cultured to 50–60% confluency on cover slips coated with poly-D-lysine and laminin (BD Biosciences). After helium/oxygen plasma treatment, cells were fixed with 4% formaldehyde and blocked in 20% fetal bovine serum (FBS) in phosphate-buffered saline (PBS). Slides were then incubated with the indicated antibodies for 30 min at 37°C , washed with PBS and incubated with an anti-rabbit IgG-FITC antibody (Molecular Probes[®]) for 1 hour. After rinsing in PBS, Hoechst 33342 was added to slides to counterstain nuclei. Slides were washed with PBS and mounted with Vectorshield (Vector laboratories, Inc. USA), and then visualized using a fluorescence microscope (Nikon Japan).

- Laroussi, M., Kong, M. G., Morfill, G. E. & Stolz, W. *Plasma Medicine* (New York: Cambridge) (2012).
- Fridman, A. & Friedman, G. *Plasma Medicine* (New York: Wiley) (2012).
- von Woedtke, T., Metelmann, H.-R. & Weltmann, K.-D. Clinical plasma medicine: State and perspectives of in vivo application of cold atmospheric plasma. *Contrib. Plasma Phys.* **54**(2), 104 (2014).
- Mai-Prochnow, A. *et al.* Atmospheric pressure plasmas: Infection control and bacterial responses. *Int. J. Antimicrob. Agents* **43**, 508 (2014).
- Arndt, S. *et al.* Cold atmospheric plasma (CAP) changes gene expression of key molecules of the wound healing machinery and improves wound healing in vitro and in vivo. *PLoS ONE* **8**, e79325 (2013).
- Emmert, S. *et al.* Atmospheric pressure plasma in dermatology: ulcer treatment and much more. *Clin. Plasma Med.* **1**, 24 (2013).
- Ishaq, M., Evans, M. & Ostrikov, K. Effect of atmospheric gas plasma on cancer cell signaling. *Int. J. Cancer* **134**, 1517 (2014).
- Stoffels, E., Sakiyama, Y. & Graves, D. B. Cold atmospheric plasma: charged species and their interactions with cells tissues. *IEEE Trans. Plasma Sci.* **36**, 1441 (2008).
- Dobrynin, D. *et al.* Physical and biological mechanisms of direct plasma interaction with living tissue. *New J. Phys.* **11**, 115020 (2009).
- Hoentsch, M. *et al.* Time-dependent effects of low-temperature atmospheric-pressure argon plasma on epithelial cell attachment, viability and tight junction formation in vitro. *J. Phys. D: Appl. Phys.* **45**, 025206 (2012).
- Blackert, S. *et al.* Influence of non-thermal atmospheric pressure plasma on cellular structures and processes in human keratinocytes (HaCaT). *J. Dermatol. Sci.* **70**, 173 (2013).
- Choi, J.-H. & Kim, G.-C. *et al.* Treatment with low-temperature atmospheric pressure plasma enhances cutaneous delivery of epidermal growth factor by regulating E-cadherin-mediated cell junctions. *Arch. Dermatol. Res.* DOI 10.1007/s00403-014-1463-9 (Online first publication) (2014).
- Kim, C.-H. Induction of cell growth arrest by atmospheric non-thermal plasma in colorectal cancer cells. *J. Biotechnol.* **150**, 530 (2010).
- Kalghatgi, S. *et al.* Effects of non-thermal plasma on mammalian cells. *PLoS ONE* **6**, e16270 (2011).
- Kim, W., Woo, K. C., Kim, G.-C. & Kim, K.-T. Nonthermal-plasma-mediated animal cell death. *J. Phys. D: Appl. Phys.* **44**, 013001 (2011).
- Joh, H. M., Kim, S. J., Chung, T. H. & Leem, S. H. Reactive oxygen species-related plasma effects on the apoptosis of human bladder cancer cells in atmospheric pressure pulsed plasma jets. *Appl. Phys. Lett.* **101**, 053703 (2012).
- Vandamme, M. *et al.* ROS implication in a new antitumor strategy based on non-thermal plasma. *Int. J. Cancer* **130**, 2185 (2012).
- Yan, X. *et al.* Plasma-induced death of HepG2 cancer cells: Intracellular effects of reactive species. *Plasma Process. Polym.* **9**, 59 (2012).
- Keidar, M. *et al.* Cold atmospheric plasma in cancer therapy. *Phys. Plasmas* **20**, 057101 (2013).
- Barekzi, N. & Laroussi, M. Effects of low temperature plasmas on cancer cells. *Plasma Process. Polym.* **10**, 1039 (2013).
- Pelicano, H., Carney, D. & Huang, P. ROS stress in cancer cells and therapeutic implications. *Drug Resist. Updat.* **7**, 97 (2004).
- Trachootham, D., Alexandre, J. & Huang, P. Targeting cancer cells by ROS-mediated mechanisms: a radical therapeutic approach? *Nat. Rev. Drug Discov.* **8**, 579 (2009).
- Han, X. *et al.* DNA damage in oral cancer cells induced by nitrogen atmospheric pressure plasma jets. *Appl. Phys. Lett.* **102**, 233703 (2013).
- Joh, H. M., Kim, S. J., Chung, T. H. & Leem, S. H. Comparison of characteristics of atmospheric pressure plasma jets using different working gases and applications to plasma-cancer cell interactions. *AIP Advances* **3**, 092128 (2013).
- Kim, S. J., Joh, H. M. & Chung, T. H. Production of intracellular reactive oxygen species and change of cell viability induced by atmospheric pressure plasma in normal and cancer cells. *Appl. Phys. Lett.* **103**, 153705 (2013).
- Kim, J. Y., Lee, D.-H., Ballato, J., Cao, W. & Kim, S.-O. Reactive oxygen species controllable non-thermal helium plasmas for evaluation of plasmid DNA strand breaks. *Appl. Phys. Lett.* **101**, 224101 (2012).
- Johnson, T. M. *et al.* Reactive oxygen species are downstream mediators of p53-dependent apoptosis. *Proc. Natl. Acad. Sci.* **93**, 11848 (1996).
- Kulms, D. *et al.* DNA damage, death receptor activation and reactive oxygen species contribute to ultraviolet radiation-induced apoptosis in an essential and independent way. *Oncogene* **21**(38), 5844 (2002).
- Weltmann, K.-D. & von Woedtke, T. Basic requirements for plasma sources in medicine. *Eur. Phys. Appl. Phys.* **55**, 13807 (2011).
- Park, H. S., Chung, T. H. *et al.* Optical and electrical characterization of an atmospheric pressure microplasma jet with a capillary electrode. *Phys. Plasmas* **17**, 033502 (2010).
- Walsh, J. L., Liu, D. X., Iza, F., Rong, M. Z. & Kong, M. G. Contrasting characteristics of sub-microsecond pulsed atmospheric air and atmospheric pressure helium-oxygen glow discharge. *J. Phys. D: Appl. Phys.* **43**, 032001 (2010).
- Thiyagarajan, M., Sarani, A. & Nicula, C. Optical emission spectroscopic diagnostics of a non-thermal atmospheric pressure helium-oxygen plasma jet for biomedical applications. *J. Appl. Phys.* **113**, 233302 (2013).
- Babaeva, N. Y. & Kushner, M. J. Interaction of multiple atmospheric-pressure micro-plasma jets in small arrays: He/O₂ into humid air. *Plasma Sources Sci. Technol.* **23**, 015007 (2014).
- Zhang, X., Huang, J., Liu, X., Peng, L., Guo, L., Lv, G., Chen, W., Feng, K. & Yang, S.-Z. Treatment of *Streptococcus mutans* bacteria by a plasma needle. *J. Appl. Phys.* **105**, 063302 (2009).
- Bairong, W., Wencho, Z. & Yikang, P. Observation of the Emission Spectra of an Atmospheric Pressure Radio-frequency Plasma Jet. *Plasma Sci. Technol.* **7**, 3045 (2005).
- Graves, D. B. The emerging role of reactive oxygen and nitrogen species in redox biology and some implications for plasma applications to medicine and biology. *J. Phys. D: Appl. Phys.* **45**, 263001 (2012).
- Cheng, T. J., Kao, H. P., Chan, C. C. & Chang, W. P. Effects of ozone on DNA single-strand breaks and 8-oxoguanine formation in A549 cells. *Environ. Res.* **93**, 279 (2003).
- Kim, G. J., Kim, W., Kim, K. T. & Lee, J. K. DNA damage and mitochondria dysfunction in cell apoptosis induced by nonthermal air plasma. *Appl. Phys. Lett.* **96**, 021502 (2010).
- Zhang, Y. T. & He, J. Frequency effects on the production of reactive oxygen species in atmospheric radio frequency helium-oxygen discharges. *Phys. Plasmas* **20**, 013502 (2013).
- Park, G. Y., Hong, Y. J., Lee, H. W., Sim, J. Y. & Lee, J. K. A Global Model for the Identification of the Dominant Reactions for Atomic Oxygen in He/O₂ Atmospheric-Pressure Plasmas. *Plasma Process. Polym.* **7**, 282 (2010).
- Staack, D., Farouk, B., Gutsol, A. & Fridman, A. DC normal glow discharges in atmospheric pressure atomic and molecular gases. *Plasma Sources Sci. Technol.* **17**, 025013 (2008).
- Pagnon, D. *et al.* On the use of actinometry to measure the dissociation in O₂ DC glow discharge: determination of the wall recombination probability. *J. Phys. D: Appl. Phys.* **28**, 1856 (1995).
- Leveille, V. & Coulombe, S. Design and preliminary characterization of a miniature pulsed RF APGD torch with downstream injection of the source of reactive species. *Plasma Sources Sci. Technol.* **14**, 467 (2005).
- Liu, D.-X., Rong, M.-Z., Wang, X.-H., Iza, F., Kong, M. G. & Bruggeman, P. Main Species and Physicochemical Processes in Cold Atmospheric-pressure He + O₂ Plasmas. *Plasma Process. Polym.* **7**, 846 (2010).
- Ershov, A. & Borysow, J. Atomic oxygen densities in a downstream microwave O₂/Ar plasma source. *Plasma Sources Sci. Technol.* **16**, 798 (2007).
- Niemi, K. *et al.* Diagnostic based modeling for determining absolute atomic oxygen densities in atmospheric pressure helium-oxygen plasma. *Appl. Phys. Lett.* **95**, 151504 (2009).
- Park, G. Y., Lee, H. W., Kim, G.-C. & Lee, J. K. Global Model of He/O₂ and Ar/O₂ Atmospheric Pressure Glow Discharges. *Plasma Process. Polym.* **5**, 569 (2008).
- Knake, N., Niemi, K., Reuter, S., Gathen, V. S. & Winter, J. Absolute atomic oxygen density profiles in the discharge core of a microscale atmospheric pressure plasma jet. *Appl. Phys. Lett.* **93**, 131503 (2008).
- Kang, S. U. *et al.* Nonthermal plasma induces head and neck cancer cell death: the potential involvement of mitogen-activated protein kinase-dependent mitochondrial reactive oxygen species. *Cell Death Dis.* **5**, e1056 (2014).



50. Zhu, H., Shertzer, H. G. *et al.* Oxidation pathways for the intracellular probe 2', 7'-dichlorofluorescein. *Arch. Toxicology* **68**, 582 (1994).

Acknowledgments

This work was supported by the National Research Foundation of Korea under Contract No. 2012R1A1A2002591 and 2013R1A2A2A04008115. This study was also supported by a grant from the National R&D Program for Cancer Control, Ministry of Health & Welfare, Republic of Korea (1420070).

Author contributions

H.M.J. conceived and designed the experiments, performed research, analyzed the data and wrote the manuscript. S.J.K. provided assistance with designing plasma diagnostics, cell experiments, and intracellular ROS assay and assisted in manuscript writing. J.Y.C. provided assistance with designing DNA damage assays and writing the manuscript. T.H.C. and T.K. conceived and supervised the study/project, provided assistance in manuscript writing.

Additional information

Supplementary information accompanies this paper at <http://www.nature.com/scientificreports>

Competing financial interests: The authors declare no competing financial interests.

How to cite this article: Joh, H.M., Choi, J.Y., Kim, S.J., Chung, T.H. & Kang, T.-H. Effect of additive oxygen gas on cellular response of lung cancer cells induced by atmospheric pressure helium plasma jet. *Sci. Rep.* **4**, 6638; DOI:10.1038/srep06638 (2014).



This work is licensed under a Creative Commons Attribution-NonCommercial-NoDerivs 4.0 International License. The images or other third party material in this article are included in the article's Creative Commons license, unless indicated otherwise in the credit line; if the material is not included under the Creative Commons license, users will need to obtain permission from the license holder in order to reproduce the material. To view a copy of this license, visit <http://creativecommons.org/licenses/by-nc-nd/4.0/>